Introduction to the parton and hadron cascade model PACIAE 3.0

An-Ke Lei,[1] Yu-Liang Yan,[2,*] Dai-Mei Zhou,[1,†] Zhi-Lei She,[3] Liang Zheng,[4] Gao-Chan Yong,[5,6] Xiao-Mei Li,[2] Gang Chen,[4] Xu Cai,[1] and Ben-Hao Sa[1,2,‡]

[1]*Key Laboratory of Quark and Lepton Physics (MOE) and Institute of Particle Physics, Central China Normal University, Wuhan 430079, China*

[2]*China Institute of Atomic Energy, P. O. Box 275 (10), Beijing 102413, China*

[3]*School of Mathematical and Physical Sciences, Wuhan Textile University, Wuhan 430200, China*

[4]*School of Mathematics and Physics, China University of Geosciences (Wuhan), Wuhan 430074, China*

[5]*School of Nuclear Science and Technology, University of Chinese Academy of Sciences, Beijing 100049, China*

[6]*Institute of Modern Physics, Chinese Academy of Sciences, Lanzhou 730000, China*

(Received 12 September 2023; revised 31 October 2023; accepted 21 November 2023; published 21 December 2023)

We develop a parton and hadron cascade model PACIAE 3.0 based on PYTHIA 6.428 and the PACIAE 2.2 program series for nuclear collisions. The original simulation framework composed of the initial partonic state, the partonic rescattering stage, hadronization stage, and the hadronic rescattering stage, is renamed a C-simulation framework for high-energy ($\sqrt{s_{NN}} \geqslant 3$ GeV) nuclear collisions. A B-simulation framework without partonic rescattering is designed for the high-energy nuclear collisions, too. In addition, an A-simulation framework is introduced for the low-energy ($\sqrt{s_{NN}} < 3$ GeV) nuclear collisions, which is developed in the hadronic degree of freedom only. In the C-simulation framework, the parton-parton inelastic-scattering processes are implemented, the single-string structure and multiple-string interaction mechanisms are proposed to investigate the strangeness enhancement, and the phenomenological coalescence hadronization model is modified. With the model, the particle yield, transverse momentum distribution, and rapidity distribution resulted from A-simulation framework well reproduce the data measured at the FOPI and E895 experiments, and the results from B- and C-simulation frameworks are well consistent with the data measured at the energies of the BNL Relativistic Heavy Ion Collider and the Large Hadron Collider.

DOI: 10.1103/PhysRevC.108.064909

I. INTRODUCTION

The phenomenological model-based Monte Carlo simulation is a powerful tool to investigate the relativistic nuclear collisions and quark gluon plasma (QGP) phase transition observed there. To this end, various models have been developed, such as PYTHIA [1,2], HERWIG [3], SHERPA [4], PCM [5], HIJING [6], QGSM [7], UrQMD [8], AMPT [9], PACIAE [10], THERMINATOR [11], PHSD [12], EPOS-LHC [13], SMASH [14], JETSCAPE [15] and ANGANTYR [16] in the high-energy sector. At low energy, the BUU-like models (such as BLOB, BUU-VM, DJBUU, GiBUU, IBL, IBUU, LBUU, PBUU, PHSD, RBUU, RVUU, SMASH, SME, χBUU, and the QMD-like models (e.g., AMD, AMD + JAM, BQMD, COMD, IMQMD, IQMD-BNU, IQMD-SINAP, JAM, JQMD, LQMD, TUQMD/DCQMD, UrQMD) are developed, cf. Refs. [17–19] and references therein.

PACIAE 3.0 is a parton and hadron cascade phenomenological model based on PYTHIA [1] and PACIAE 2.2 series [10,20–23]. The PACIAE model is developed from the LUCIAW [24–26] and JPCIAE [27] models. The LUCIAE model was based on the FRITIOF model [28] with the extension of implementing both the FIRECRACKER model (collective multigluon emission in the interacting string color field) and the hadronic rescattering. The JPCIAE model was based on the JETSET and PYTHIA models [29], being able to simulate the relativistic hadron-hadron and heavy-ion collisions. Soon after, the JETSET model had been blended in PYTHIA, and the JPCIAE was renamed PACIAE 1.0 correspondingly. As quoted in Ref. [30], not only the LUCIAE model but also the JPCIAE (PACIAE 1.0) model and even the PACIAE 3.0 model are all based on the Lund string fragmentation (LSF) regime.

Relative to the old version, PACIAE 3.0 has the following new features:

(1) The original simulation framework composed of the initial partonic state, the partonic rescattering stage, hadronization stage, and the hadronic rescattering stage is renamed the C-simulation framework for high-energy ($\sqrt{s_{NN}} \geqslant 3$ GeV) nuclear collisions, as shown in the right part of Fig. 1. Simultaneously, we construct a B-simulation framework for high-energy nuclear collisions, too, in which the partonic rescattering is not

*yanyl@ciae.ac.cn
†zhoudm@mail.ccnu.edu.cn
‡sabh@ciae.ac.cn

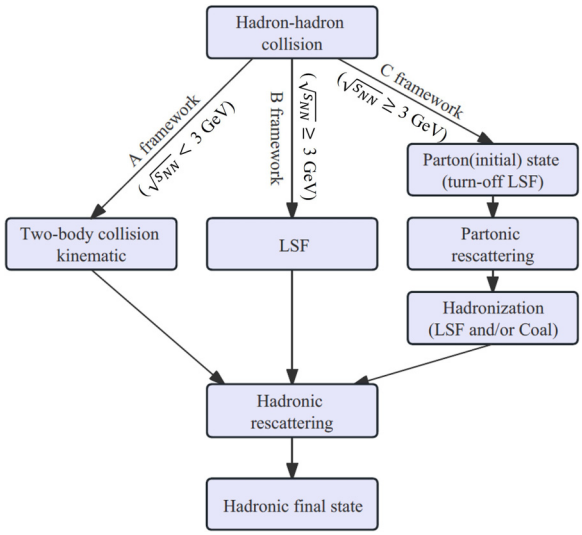

FIG. 1. A sketch of the hadron-hadron collision (LSF: Lund string fragmentation, Coal: coalescence).

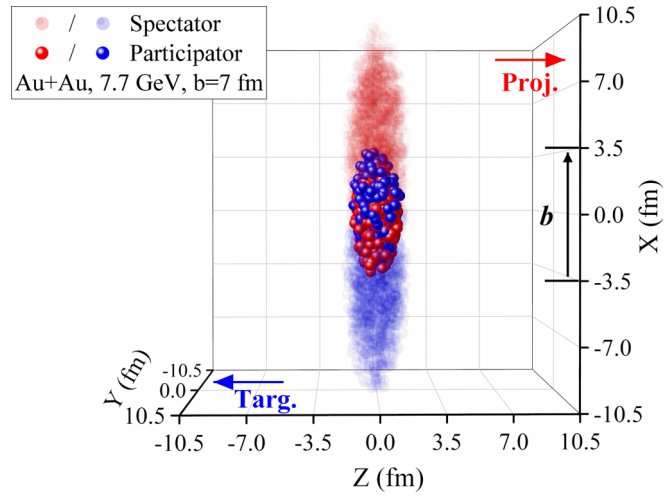

FIG. 2. The initial spatial distribution of nucleons in the impact parameter $b = 7$ fm Au + Au collisions at $\sqrt{s_{NN}} = 7.7$ GeV after Lorentz contraction.

contained compared with C-simulation framework, as shown in the middle part of Fig. 1. Additionally, an A-simulation framework developing in the hadronic degree of freedom only is introduced for the low-energy ($\sqrt{s_{NN}} < 3$ GeV) nuclear collisions, as shown in the left part of Fig. 1.

(2) In the C-simulation framework, the single-string structure and multiple-string interaction mechanisms are introduced to investigate the strangeness enhancement.

(3) The parton-parton inelastic-scattering processes are implemented in the partonic rescattering stage in C-simulation framework.

(4) In the C-simulation framework, the phenomenological coalescence hadronization model is modified.

(5) The *hh* total cross section is assumed to be proportional to the nucleon-nucleon (*NN*) total cross section with coefficient equal to the ratio of effective valence quark number in *hh* collision system to that in *NN* collision system [30,31]. And the experimentally measured *NN* total cross section [32] is adopted in the A-, B-, and C-simulation frameworks.

The PACIAE 3.0 program is now available on the open source platforms GitHub [33] and Gitee [34].

II. CUMULATIVE SUPERPOSITION OF HADRON-HADRON COLLISIONS

To begin with a heavy-ion collision simulation one first distributes the nucleons in its own nucleus sphere by the Woods-Saxon distribution (for radius r) and the uniform distribution in 4π solid angle (for direction). The time origin is set at the moment of two centers of the projectile and target spheres have the same coordinates of $z = 0$ [10,21,35].

Taking the Au + Au collision at $\sqrt{s_{NN}} = 7.7$ GeV with the impact parameter $b = 7$ fm as an example, the initial momentum of each nucleon in the projectile nucleus (Proj.) is $p_x = p_y = 0$ and $p_z = p_{\rm beam}$, and is $p_x = p_y = 0$ and $p_z = -p_{\rm beam}$ in the target nucleus (Targ.). The Lorentz contraction is then performed. Figure 2 shows the initial spatial distribution of nucleons after Lorentz contraction. Meanwhile, the initial particle list, composed of four spatial and four-momentum vectors of all nucleons in the Au + Au collision system, is constructed.

We assume the particle trajectory in the velocity field of a nuclear collision system is a straight line. Two particles i and j may collide if their minimum approaching distance D satisfies [10]

$$D \leqslant \sqrt{\sigma^{\rm tot}/\pi}, \tag{1}$$

where $\sigma^{\rm tot}$ refers to the total cross section of two particles. The collision time t_{ij} is then calculated [10]. Here for the nucleon-nucleon collisions, the cross section $\sigma^{\rm tot}_{NN}$ is adopted.

Two circulation loops are set: one for i cycling over all the projectile nucleons, another one for j cycling over all the target nucleons. With the calculated collision time t_{ij} of all i-j pairs the initial *NN* collision time list is constructed for a heavy-ion collision system.

An *NN* collision with the least collision time is selected from the list. If it is properly executed (see next section) its final hadronic state is available and the generated hadrons (including leading nucleons) are counted as its contribution to the final hadronic state of the heavy-ion collision. The particle (nucleon or hadron) list is then updated by removing two colliding particles from the particle list and adding the generated particles to the particle list. Consequently, the *NN* (*hh*) collision time list is updated by removing the *NN* (*hh*) collision pair containing any one of the colliding particles from the old collision time list and adding the new collision pairs composed of one particle from the generated particles and another one from the old particle list.

A new *NN* (*hh*) collision with the least collision time is then selected from the updated collision time list and properly executed. With repeating the aforementioned steps until the

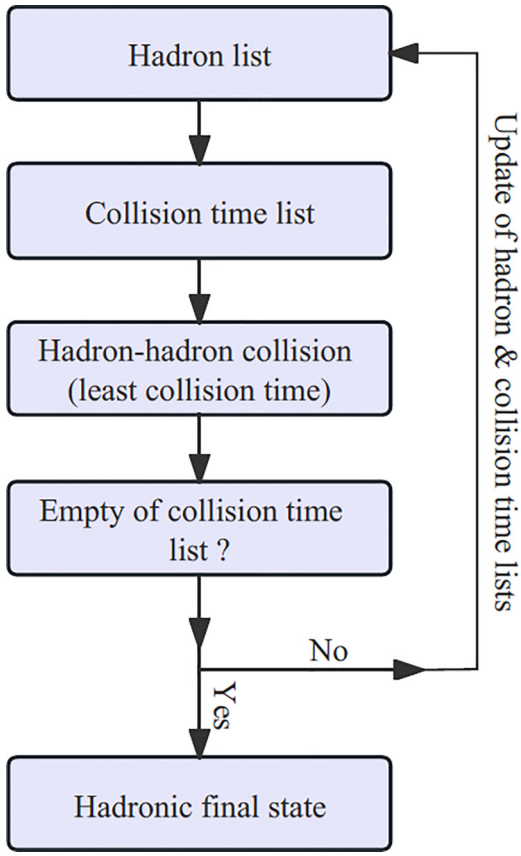

FIG. 3. Sketch for superposition of hadron-hadron collisions.

particle collision time list is empty, a Monte Carlo simulation for a heavy-ion collision is finished.

Therefore, in the PACIAE model, a heavy-ion collision is indeed described as a cumulative superposition (CS) of the NN (hh) collisions, i.e., the produced hadrons (including leading nucleons) will join in the processes of updating hadron list and hh collision time list, as shown in Fig. 3. One can refer to the program file parini_30.f for the details.

III. MODEL FOR HADRON-HADRON COLLISION

The last section is common for the A-, B-, and C-simulation frameworks but leaves a problem of the hh collision execution. It will be addressed in this section for A-, B-, and C-simulation frameworks, individually.

The hh collision in the A-simulation framework is described by the two-body elastic and inelastic-scattering kinematics in hadronic degree of freedom [2], as shown in the left part of Fig. 1.

Up to the second time of updating collision list, the inelastic scattering is restricted to the following processes:

$$
\begin{aligned}
&p+p\to\Delta^{+}+p, \quad p+p\to\Delta^{++}+n,\\
&p+n\to\Delta^{+}+n, \quad p+n\to\Delta^{0}+p,\\
&n+n\to\Delta^{0}+n, \quad n+n\to\Delta^{-}+p,\\
&\Delta^{+}+p\to p+p, \quad \Delta^{+}+n\to p+n,\\
&\Delta^{0}+p\to p+n, \quad \Delta^{0}+n\to n+n,\\
&\Delta^{++}+n\to p+p, \quad \Delta^{-}+p\to n+n,\\
&\pi^{-}+p\to\Delta^{-}+\pi^{+}, \quad \pi^{-}+p\to\rho^{0}+n,\\
&\pi^{-}+p\to\rho^{-}+p, \quad \pi^{-}+p\to\Delta^{+}+\pi^{-},\\
&\pi^{-}+p\to\Delta^{0}+\pi^{0}, \quad \pi^{-}+n\to\Delta^{-}+\pi^{0},\\
&\pi^{-}+n\to\rho^{-}+n, \quad \pi^{-}+n\to\Delta^{0}+\pi^{-},\\
&\pi^{+}+p\to\Delta^{++}+\pi^{0}, \quad \pi^{+}+p\to\Delta^{+}+\pi^{+},\\
&\pi^{+}+p\to\rho^{+}+p, \quad \pi^{+}+n\to\Delta^{++}+\pi^{-},\\
&\pi^{+}+n\to\Delta^{0}+\pi^{+}, \quad \pi^{+}+n\to\Delta^{+}+\pi^{0},\\
&\pi^{+}+n\to\rho^{0}+p, \quad \pi^{+}+n\to\rho^{+}+n.
\end{aligned}
$$

For both the elastic- and inelastic-scattering processes, the four-momenta of scattered hadrons are determined by the energy-momentum conservation [10]. Among the inelastic-scattering processes, if it is an exothermic reaction, such as $p+p\to\Delta^{+}+p$, the threshold energy effect is taken into account. For an exothermic inelastic scattering, if the kinetic energy of its incident channel is less than the threshold energy, it should be dealt with as an elastic scattering rather than inelastic scattering originally. Here two parameters are essential: One is the ratio of inelastic cross section to total cross section $R_{\mathrm{inela/tot}}$ ("x_ratio" in program). Another is the Δ particle instantaneously decay probability ("decpro") at the moment of formation.

Inspired by the additive quark model [31], we assume different outgoing channels and the resonance production process developed from a given incident channel are equally distributed. Up to the second time of updating the collision list, there is only one resonance process of $p+\pi^{+}\to\Delta^{++}$ to be considered.

In the PACIAE model, the experimental data of $\sigma_{NN}^{\mathrm{tot}}\approx 70$ mb measured at the Large Hadron Collider (LHC) energies and $\sigma_{NN}^{\mathrm{tot}}\approx 40$ mb measured at energies of the BNL Relativistic Heavy Ion Collider (RHIC) and below are adopted [32]. The total cross section of IJ collision (hadron I bombards with J), is assumed to be proportional to the NN collision cross section, with the coefficient calculated by [2,31]

$$C_{IJ}=\frac{n_{\mathrm{eff}}^{I}n_{\mathrm{eff}}^{J}}{n_{\mathrm{eff}}^{N}n_{\mathrm{eff}}^{N}}, \tag{2}$$

$$n_{\mathrm{eff}}^{I}=n_{d}^{I}+n_{u}^{I}+0.6n_{s}^{I}+0.2n_{c}^{I}+0.07n_{b}^{I}. \tag{3}$$

In above equation, n_{i}^{I} refers to the number of effective ith valence quark (antiquark) in the Ith hadron.

Differently, in the high-energy B-simulation framework, each hh collision is executed by PYTHIA [1], resulting in a final hadronic state composed of a lot of produced hadrons (including the leading hadrons) with their four-momenta. The four spatial coordinates of produced hadrons are assumed to be randomly distributed between two colliding hadrons in each direction individually. Figure 4 without the partonic rescattering (PRS) and hadronic rescattering (HRS) (along with the middle part of Fig. 1 without HRS) is just a sketch for the execution of a pp collision in PYTHIA: As a proton consists of three valence quarks, countless sea quarks and gluons, a pp collision, may comprise n_{MPI} parton-parton pair interactions. Here n_{MPI} refers to the number of multiparton

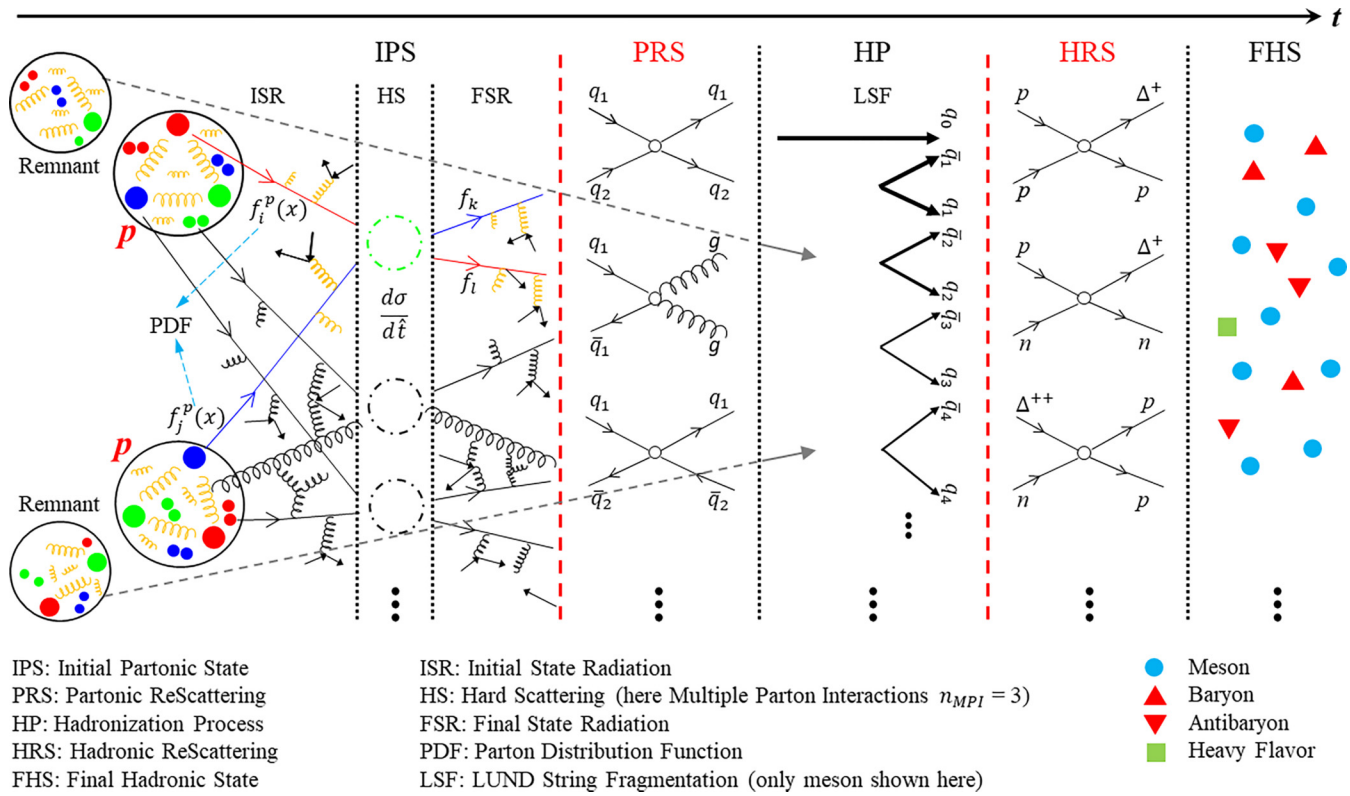

FIG. 4. Sketch for the physical routines in a high-energy pp simulation.

interactions (MPIs). Each parton-parton collision is described by a hard scattering (HS) together with the initial-state radiation (ISR, or initial-state parton shower) and final-state radiation (FSR, or final-state parton shower). The resulted partons then hadronize together with two remnants providing the final hadronic state for a pp collision.

The hadronization in the PYTHIA model is phenomenologically described by the string iterative breaking processes: In case of the iterative string breaking process starts at the q_0 end of a $q_0\bar{q}_0$ string, if the string energy is large enough, a new $q_1\bar{q}_1$ pair may be excited from the vacuum such that a meson of $q_0\bar{q}_1$ may be formed and left behind the quark q_1. Later on, the q_1 quark in its turn may excite a $q_2\bar{q}_2$ pair from the vacuum and combines another meson together with the $\bar{q}_2$. Repeating this breaking process, a lot of mesons are formed in the final hadronic state of the hh collision system, as shown in Fig. 5.

Figure 6, taken from Ref. [2], shows the baryon (antibaryon) generation process in the popcorn model [2]: One starts from a red-antired ($r\bar{r}$) string [with color flow indicated by the arrow in Fig. 6(a)]. A green-antigreen ($g\bar{g}$) pair may be excited from vacuum between $r\bar{r}$ reversing the color flow in the central part of the string [Fig. 6(b)]. A third blue-antiblue ($b\bar{b}$) pair is created and breaks the string into two [Fig. 6(c)]. Then another string-breaking process happens and produces a $b\bar{b}$ meson between the baryon (rgb) and antibaryon ($\bar{b}\bar{g}\bar{r}$).

Taking meson production as an example, once the $q_{i\text{-}1}$ and $\bar{q}_i$ flavors are sampled, a selection should be made between the possible multiplets. The different multiplets have different relative composition probability, which is not given by first principle but must depend on the fragmentation processes, cf. Ref. [1] for the details.

In the C-simulation framework, each hh is also executed by PYTHIA [1] but with presetting of the hadronization turning-off. After the execution, the breaking-up of the strings and diquarks would be made to result in an initial partonic state which consists of numerous produced partons (including

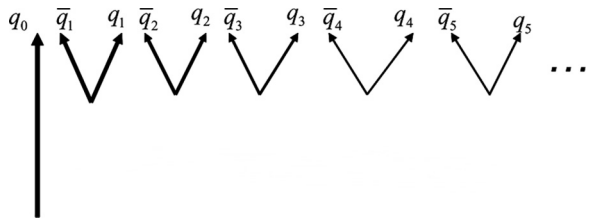

FIG. 5. Feynman-diagram-like sketch for the string iterative breaking processes starting from the quark end of a $q_0\bar{q}_0$ string.

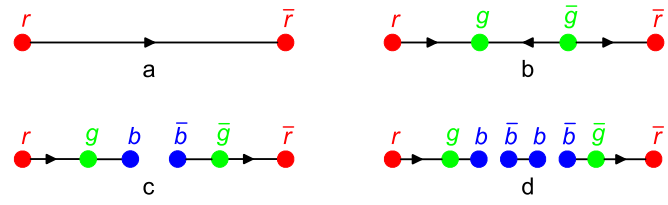

FIG. 6. The stepwise sketch illustrating the popcorn production of a baryon-antibaryon pair in the string iterative breaking processes, taken from Ref. [2].

TABLE I. Parton-parton collisions.

Order	Process	$\lvert\overline{M}\rvert^2$
1	$q_1q_2 \to q_1q_2$	$\frac{4}{9}\frac{s^2+u^2}{t^2}$
2	$q_1q_1 \to q_1q_1$	$\frac{4}{9}\left(\frac{s^2+u^2}{t^2}+\frac{s^2+t^2}{u^2}\right)-\frac{8}{27}\frac{s^2}{ut}$
3	$q_1\bar{q}_2 \to q_1\bar{q}_2$	$\frac{4}{9}\frac{s^2+u^2}{t^2}$
4	$q_1\bar{q}_1 \to q_2\bar{q}_2$	$\frac{4}{9}\frac{t^2+u^2}{s^2}$
5	$q_1\bar{q}_1 \to q_1\bar{q}_1$	$\frac{4}{9}\left(\frac{s^2+u^2}{t^2}+\frac{t^2+u^2}{s^2}\right)-\frac{8}{27}\frac{u^2}{ts}$
6	$q\bar{q} \to gg$	$\frac{32}{27}\frac{u^2+t^2}{ut}-\frac{8}{3}\frac{u^2+t^2}{s^2}$
7	$gg \to q\bar{q}$	$\frac{1}{6}\frac{u^2+t^2}{ut}-\frac{3}{8}\frac{u^2+t^2}{s^2}$
8	$qg \to qg$	$-\frac{4}{9}\frac{u^2+s^2}{us}+\frac{u^2+s^2}{t^2}$
9	$gg \to gg$	$\frac{9}{2}\left(3-\frac{ut}{s^2}-\frac{us}{t^2}-\frac{st}{u^2}\right)$

the quark constituents of leading hadrons) with their four-momenta. The four spatial coordinates of produced partons are assumed to be randomly distributed between two colliding hadrons in each direction individually. This partonic state then undergoes the partonic rescattering, where the lowest-order perturbative quantum chromodynamics (LO-pQCD) parton-parton interaction cross section [36,37] is employed. After partonic rescattering the hadronization is implemented by the Lund string fragmentation regime and/or the coalescence model (see Sec. VII) to generate an intermediate hadronic state. It is composed of a lot of produced hadrons with their four-momenta. The four spatial coordinates of produced hadrons are assumed to be randomly distributed between two colliding hadrons in each direction individually. The hadronic rescattering is then followed resulting in a final hadronic state for a *hh* collision system. Meanwhile, the C-simulation framework could be selected to stop at any stage desired conveniently. Figure 4, along with the right part of Fig. 1, shows the above physical processes in a C-framework *pp* simulation. As for the details, one can refer to the program file parini_30.f.

IV. PARTONIC RESCATTERING IN C-SIMULATION FRAMEWORK

In the partonic rescattering stage, we only consider parton $2 \to 2$ processes. There are nine parton $2 \to 2$ processes, given in the Table I together with their differential cross section expressed in the form of

$$\frac{d\sigma}{dt}(ab \to cd; s, t) = K\frac{\pi\alpha_s^2}{s^2}|\overline{M}(ab \to cd)|^2, \tag{4}$$

which is calculated by the LO-pQCD approximation [36,37]. In the equation above the α_s refers to strong-coupling factor. The s, t, and u (cf. Table I) are the Mandelstam invariants in the kinematics of $ab \to cd$ quark process. And K is an enlarged factor introduced empirically. The corresponding integral cross section is

$$\frac{d\sigma}{dt}(ab \to cd; s) = \int_{-s}^{0}\frac{d\sigma}{dt}(ab \to cd; s, t)dt. \tag{5}$$

As the differential cross section is divergent at $t \to 0$, Debye screening coefficient μ has to be introduced. Therefore, taking the number 1 process in Table I as an example, its matrix element in differential cross section should be modified to

$$|M(q_1q_2 \to q_1q_2)|^2 = \frac{4}{9}\frac{s^2+u^2}{t^2-\mu^2}. \tag{6}$$

Among the listed parton-parton collisions in Table I, the number 1, 2, 3, 5, 8, and 9 processes are elastic-scattering processes. In the elastic-scattering process, as quark flavors in incident and outgoing channels are unchanged, it is easy to handle. Most of the parton and hadron transport models, like AMPT [9] and PACIAE 2.2, only take elastic parton-parton scattering processes into account. In PACIAE 3.0, the number 4, 6, and 7 inelastic parton-parton scattering processes are implemented.

In the number 4 and 7 inelastic-scattering processes, if the invariant mass of incident channel is large enough, the available outgoing flavor may be different. We assume the different outgoing flavor is distributed inversely proportional to the xth power of its respective constituent quark masses ($p_q \propto m_q^{-x}$). Here x is a parameter has yet to fix by fitting the experimental data (default, $D = 3.65$).

With the parton-parton differential cross section of Eq. (4) and integral cross section of Eq. (5) the partonic rescattering can be simulated as follows: We first construct an initial parton-parton collision time list based on the parton list (in the initial partonic state), the parton-parton differential cross section, and the integral cross section. Second, a parton-parton collision with least collision time is selected from parton-parton collision time list and properly implemented. Third, the parton list and parton-parton collision time list are updated. A new parton-parton collision with least collision time is then selected from the updated collision time list and properly executed. By repeating the aforementioned steps until the parton-parton collision time list is empty, the Monte Carlo simulation for the partonic rescattering is finished. See the program file parcas_30.f for details.

V. HADRONIC RESCATTERING

The simulation framework of hadronic rescattering is similar to the one in the Sec. II. However, here we first filter out the desired hadrons from the available hadron list after hadronization to construct an initial hadron list. Then we construct a hadronic collision time list, select a *hh* collision pair with least collision time and execute it properly, update hadron list and hadronic collision time list, etc., one step after another, like that in the Sec. II. One can refer to the program file hadcas_30.f for details.

Here the *NN* total cross section is also taken from experiment and the total cross section of *IJ* incident channel is assumed to be proportional to the *NN* one with the coefficient given by Eq. (2). The ratio of inelastic to total cross section (x_ratio in the program, $D = 0.85$) is a model parameter, too.

In the hadronic rescattering we consider nearly 600 different inelastic *hh* collisions (cf. program file hadcas_30.f),

besides the elastic *hh* collision. The inelastic *hh* collisions listed at the begin of Sec. III, for instance, are the main parts of them. If the user-desired channel is not in the 600 list, it has to be added manually.

VI. STRANGENESS ENHANCEMENT

In the string fragmentation picture of the relativistic *NN* and heavy-ion collisions, strange quark production is suppressed comparing with up and down quarks due to the tunneling probability [1]

$$P(m_{\perp q}) = \exp\left(-\frac{\pi}{\kappa}m_q^2\right)\exp\left(-\frac{\pi}{\kappa}p_{\perp q}^2\right), \tag{7}$$

where the $\kappa \approx 1$ GeV/fm $\approx 0.2\text{GeV}^2$ is the (vacuum) string tension for a pure $q\bar{q}$ string. However a pronouncing enhancement of strange particle relative to pion production is really observed by ALICE collaboration in the relativistic *pp* collisions [38]. To this end, we introduce an effective string tension stemming from single-string structure [39] and the multiple-string interaction [40,41] instead of (vacuum) string tension in Eq. (7).

In Ref. [39], we have constructed a parametrized effective string tension coming from the single-string structure:

$$\kappa_{\text{eff}}^{s} = \kappa_0(1-\xi)^{-\alpha}. \tag{8}$$

In the above equation, κ_0 is string tension of pure (dipole) $q\bar{q}$ string. α is a parameter to be tuned with experimental data. ξ is parametrized as

$$\xi = \frac{\ln\left(\frac{k_{\perp\max}^2}{s_0}\right)}{\ln\left(\frac{s}{s_0}\right) + \sum_{j=\text{gluon}}\ln\left(\frac{k_{\perp j}^2}{s_0}\right)}, \tag{9}$$

where $k_\perp$ denotes the transverse momentum of the gluons inside a dipole string. The $\sqrt{s}$ and $\sqrt{s_0}$ give the mass of the string system and the parameter related to the typical hadron mass, respectively. The ξ quantifies the difference between a gluon wrinkled string and a pure $q\bar{q}$ string. The value of this effective string tension changes on a string-by-string basis in the current implementation and takes the string-wise fluctuations into consideration.

Later on, we consider the multiple string interaction effects from the correlation of strings overlapping in a limited transverse space by parametrizing the effective string tension, in a manner similar to the close-packing strings discussed in Ref. [42] as follows:

$$\kappa_{\text{eff}}^{m} = \kappa_0\left(1 + \frac{\frac{N_{\text{coll}}}{N_{\text{part}}}n_{\text{MPI}} - 1}{1 + p_{T\ \text{ref}}^2/p_0^2}\right)^r. \tag{10}$$

In the above equation, the n_{MPI} indicates the number of multiple parton interactions in a *pp* collision system and $p_{T\ \text{ref}}^2/p_0^2$ shows the transverse scale of a typical string object relative to the proton size. The exponent r is then treated as a free parameter. As larger n_{MPI} leads to a denser string system in an event, n_{MPI} strongly correlates with the charged particle multiplicity. The factor of $N_{\text{coll}}/N_{\text{part}}$ amplifies the multiple-string interaction effects in heavy-ion collisions [41]. Multiplying κ_{eff}^{s} on both side of Eq. (10), one obtains

$$\kappa_{\text{eff}}^{s} \times \kappa_{\text{eff}}^{m} = \kappa_{\text{eff}}^{s}\left(1 + \frac{\frac{N_{\text{coll}}}{N_{\text{part}}}n_{\text{MPI}} - 1}{1 + p_{T\ \text{ref}}^2/p_0^2}\right)^r \equiv \kappa_{\text{eff}}^{s+m}. \tag{11}$$

In PYTHIA [1] the strange quark suppression relevant parameters are

(1) PARJ(1), the suppression of diquark-antidiquark pair production in string-breaking process, compared with quark-antiquark pair production.
(2) PARJ(2), the suppression of *s* quark pair production compared with *u* or *d* pair production.
(3) PARJ(3), the extra suppression of *s* diquark production compared with the normal suppression of *s* quarks.
(4) PARJ(21), the Gaussian width of the transverse momentum distribution for primary hadrons in fragmentation.

They can be related to the effective string tension through a scaling function implied by the tunneling probability:

$$\lambda_2 = \lambda_1^{\kappa_1^{\text{eff}}/\kappa_2^{\text{eff}}}. \tag{12}$$

In the above equation, $\kappa_1^{\text{eff}} = 1$ GeV/fm represents the vacuum string tension and κ_2^{eff} is the effective string tension. The λ_1 and λ_2 refer to the one among PARJ(1), PARJ(2), and PARJ(3) before and after modification, respectively. The λ_2 will be enlarged when the effective string tension κ_2^{eff} becomes greater than κ_1^{eff}.

Similarly, the PARJ(21) varies with the effective string tension as

$$\sigma_2 = \sigma_1\left(\frac{\kappa_2^{\text{eff}}}{\kappa_1^{\text{eff}}}\right)^{1/2}. \tag{13}$$

VII. PHENOMENOLOGICAL COALESCENCE HADRONIZATION MODEL

There are two hadronization mechanisms implemented in C-simulation framework: The Lund string fragmentation regime and the coalescence (hadronization) model COCCNU (CO: the moral of coalescence, CCNU: short for "Central China Normal University"). It is a phenomenological coalescence model unlike the semi-analytical coalescence models in Refs. [43–48].

In the PACIAE C-simulation framework, if the coalescence model is selected, one then starts from the parton list (composed of quarks, antiquarks, and gluons) available after partonic rescattering. All the gluons in this parton list are randomly split into quark-antiquark pairs, resulting in a new parton list composed of quarks (antiquarks) only.

Then the collision system proceeds with energetic quark (antiquark) deexcitation process: A cycle over quark (antiquark) in the parton list is constructed. If the energy of a quark (antiquark) is larger than the deexcitation threshold energy e_{she}, it deexcites according to the vacuum excitation regime of $q_0 \to q_0 q_1 \bar{q}_1$ ($\bar{q}_0 \to \bar{q}_0 q_1 \bar{q}_1$) [1]. The generated quark-antiquark pair is filled at the end of the parton list. This deexcitation process is continuously repeated until the quark (antiquark) energy goes down to e_{she}. In each step,

TABLE II. Mesons in coalescence hadronization model.

	Pseudoscalar meson			Vector meson		
Quark conf.	Name	Mass (GeV)	Proper probability	Name	Mass (GeV)	Proper probability
$u\bar{d}$	π^+	0.1396	1	ρ^+	0.7669	1
$d\bar{u}$	π^-	0.1396	1	ρ^-	0.7669	1
$u\bar{s}$	K^+	0.4936	1	K^{*+}	0.8921	1
$s\bar{u}$	K^-	0.4936	1	K^{*-}	0.8921	1
$d\bar{s}$	K^0	0.4977	1	K^{*0}	0.8962	1
$s\bar{d}$	$\bar{K}^0$	0.4977	1	$\bar{K}^{*0}$	0.8962	1
$u\bar{u}$	π^0	0.1350	0.5	ρ^0	0.7700	0.5
$u\bar{u}$	η	0.5488	0.167	ω	0.7820	0.5
$u\bar{u}$	η'	0.9575	0.333	–	–	–
$d\bar{d}$	π^0	0.1350	0.5	ρ^0	0.7700	0.5
$d\bar{d}$	η	0.5488	0.167	ω	0.7820	0.5
$d\bar{d}$	η'	0.9575	0.333	–	–	–
$s\bar{s}$	η	0.5488	0.667	ϕ	1.019	1
$s\bar{s}$	η'	0.9575	0.333	–	–	–
$c\bar{d}$	D^+	1.869	1	D^{*+}	2.010	1
$d\bar{c}$	D^-	1.869	1	D^{*-}	2.010	1
$c\bar{u}$	D^0	1.865	1	D^{*0}	2.007	1
$u\bar{c}$	$\bar{D}^0$	1.865	1	$\bar{D}^{*0}$	2.007	1
$c\bar{s}$	D_s^+	1.969	1	D_s^{*+}	2.112	1
$s\bar{c}$	D_s^-	1.969	1	D_s^{*-}	2.112	1
$c\bar{c}$	η_c	2.980	1	J/ψ	3.097	1
$u\bar{b}$	B^+	5.279	1	B^{*+}	5.325	1
$b\bar{u}$	B^-	5.279	1	B^{*-}	5.325	1
$d\bar{b}$	B^0	5.279	1	B^{*0}	5.325	1
$b\bar{d}$	$\bar{B}^0$	5.279	1	$\bar{B}^{*0}$	5.325	1
$s\bar{b}$	B_s^0	5.366	1	B_s^{*0}	5.415	1
$b\bar{s}$	$\bar{B}_s^0$	5.366	1	$\bar{B}_s^{*0}$	5.415	1
$c\bar{b}$	B_c^0	6.594	1	B_c^{*0}	6.602	1
$b\bar{c}$	$\bar{B}_c^0$	6.594	1	$\bar{B}_c^{*0}$	6.602	1
$b\bar{b}$	η_b	9.389	1	Υ	9.460	1

the transverse momenta of generated quark-antiquark pair are sampled according to the Gaussian or exponential distributions (controlled by the parameter "i_pT"). The generated quark-antiquark pair takes a part of its mother quark (antiquark) energy, the fraction of this part is sampled randomly from a uniform distribution or fragmentation functions [1] [controlled by the parameter adj1(29)]. Of course, the corresponding four-momentum should be subtracted from mother quark (antiquark). The finishing of this cycle means the end of the first generation deexcitation. Subsequently, the second generation deexcitation cycling over the generated quarks (antiquarks) will proceed. A free parameter adj1(16), $D = 1$ is set for the allowed maximum number of deexcitation generation.

In the gluon splitting and the energetic quark (antiquark) deexcitation processes, a key problem is the flavor generation probability of the outgoing channel. We assume the different outgoing flavors are distributed inversely proportional to the xth power of their respective constituent quark masses. Here the x is a parameter has yet to fix by fitting the experimental data (default is $D = 3.65$).

After the gluon splitting and the energetic quark (antiquark) deexcitation, the collision system is represented by a quark (antiquark) list. Then it proceeds to a combination loop: Selecting a proper quark and antiquark from the parton list to form a specific meson in the meson Table II, and/or choosing three quarks (antiquarks) to coalesce into a specific baryon (antibaryon) in the baryon Table III. Here many strategies are possible, for example, the combination starts from quark or antiquark, to combine into a meson or baryon, etc. Which one is better has to be decided by reproducing the

TABLE III. Baryons in coalescence hadronization model.

	Spin-parity $\frac{1}{2}^+$			Spin-parity $\frac{3}{2}^+$		
Quark conf.	Name	Mass (GeV)	Proper probability	Name	Mass (GeV)	Proper probability
ddd				Δ^-	1.234	1
ddu	n	0.9396	1	Δ^0	1.233	1
duu	p	0.9383	1	Δ^+	1.232	1
uuu	–	–	–	Δ^{++}	1.231	1
dds	Σ^-	1.197	1	Σ^{*-}	1.387	1
dus	Λ^0	1.116	0.5	–	–	–
dus	Σ^0	1.193	0.5	Σ^{*0}	1.384	1
uus	Σ^+	1.189	1	Σ^{*+}	1.383	1
dss	Ξ^-	1.321	1	Ξ^{*-}	1.535	1
uss	Ξ^0	1.315	1	Ξ^{*0}	1.532	1
sss	–	–	–	Ω^-	1.672	1
ddc	Σ_c^0	2.454	1	Σ_c^{*0}	2.518	1
duc	Λ_c^+	2.284	0.5	–	–	–
duc	Σ_c^+	2.4535	0.5	Σ_c^{*+}	2.500	1
dsc	Ξ_c^0	2.4703	0.5	–	–	–
dsc	$\Xi_c^{\prime 0}$	2.550	0.5	Ξ_c^{*0}	2.630	1
usc	Ξ_c^+	2.4656	0.5	–	–	–
usc	$\Xi_c^{\prime +}$	2.550	0.5	Ξ_c^{*+}	2.630	1
uuc	Σ_c^{++}	2.4529	1	Σ_c^{*++}	2.500	1
dcc	Ξ_{cc}^+	3.598	1	Ξ_{cc}^{*+}	3.6565	1
ucc	Ξ_{cc}^{++}	3.598	1	Ξ_{cc}^{*++}	3.6565	1
ssc	Ω_c^0	2.704	1	Ω_c^{*0}	2.800	1
scc	Ω_{cc}^0	3.7866	1	Ω_{cc}^{*0}	3.8247	1
ccc	–	–	–	Ω_{ccc}^{*++}	4.9159	1
ddb	Σ_b^-	5.800	1	Σ_b^{*-}	5.810	1
uub	Σ_b^+	5.800	1	Σ_b^{*+}	5.810	1
dub	Λ_b^0	5.641	0.5	–	–	–
dub	Σ_b^0	5.800	0.5	Σ_b^{*0}	5.810	1
dsb	Ξ_b^-	5.840	0.5	–	–	–
dsb	$\Xi_b^{\prime -}$	5.960	0.5	Ξ_b^{*-}	5.970	1
usb	Ξ_b^0	5.840	0.5	–	–	–
usb	$\Xi_b^{\prime 0}$	5.960	0.5	Ξ_b^{*0}	5.970	1
dcb	Ξ_{bc}^0	7.0057	0.5	–	–	–
dcb	$\Xi_{bc}^{\prime 0}$	7.0372	0.5	Ξ_{bc}^{*0}	7.0485	1
ucb	Ξ_{bc}^+	7.0057	0.5	–	–	–
ucb	$\Xi_{bc}^{\prime +}$	7.0372	0.5	Ξ_{bc}^{*+}	7.0485	1
dbb	Ξ_{bb}^-	10.4227	1	Ξ_{bb}^{*-}	10.4414	1
ubb	Ξ_{bb}^0	10.4227	1	Ξ_{bb}^{*0}	10.4414	1
ssb	Ω_b^-	6.120	1	Ω_b^{*-}	6.130	1
scb	Ω_{bc}^0	7.191	0.5	–	–	–
scb	$\Omega_{bc}^{\prime 0}$	7.211	0.5	$\Omega_{bc}^{\prime *0}$	7.219	1
sbb	Ω_{bb}^-	10.6021	1	Ω_{bb}^{*-}	10.6143	1
ccb	Ω_{bcc}^+	8.3095	1	Ω_{bcc}^{*+}	8.3133	1
cbb	Ω_{bbc}^0	11.7077	1	Ω_{bbc}^{*0}	11.7115	1
bbb	–	–	–	Ω_{bbb}^{*-}	15.1106	1

TABLE IV. The midrapidity charged particle multiplicity density $dN_{ch}/d\eta$ in 0%–6% most central Au + Au collisions at $\sqrt{s_{NN}} = 0.2$ TeV for $|\eta| < 1$ from PHOBOS [51] and 0%–5% most central Pb + Pb collisions at $\sqrt{s_{NN}} = 2.76$ TeV for $|\eta| < 0.5$ from ALICE [52] compared with the results from PACIAE 3.0 B-framework and C-framework with LSF as well as C-framework with Coal.

System	$\sqrt{s_{NN}}$ (TeV)	Expt.	B-framework	C-framework LSF	C-framework Coal
Au + Au	0.2	1310 ± 69[a]	1283	1301	1288
Pb + Pb	2.76	1610 ± 60[b]	1667	1672	1587

[a]Taken from PHOBOS [51].
[b]Taken from ALICE [52].

experimental data. Presently, the combination starts from antiquark in PACIAE 3.0. A selected antiquark is assumed to form an antibaryon together with two other antiquarks by probability p and to form a meson together with a quark by probability $(1-p)$. In this work we introduce the antibaryon suppression factor

$$\text{adj1(31)} = \frac{N_{\bar{b}}}{N_m} \tag{14}$$

relative to meson, where $N_{\bar{b}}$ (N_m) refers to the multiplicity of antibaryon (meson) generated in a simulated event. Then we relate it to p as follows:

$$p = \frac{N_{\bar{b}}}{N_m + N_{\bar{b}}} = \frac{N_{\bar{b}}/N_m}{1 + N_{\bar{b}}/N_m} = \frac{\text{adj1(31)}}{1 + \text{adj1(31)}}. \tag{15}$$

If the selected antiquark is $\bar{s}$, an extra suppression factor adj1(33) for strange antibaryon relative to strange meson should be introduced multiplying on adj1(31) in both the numerator and denominator in Eq. (15) to obtain

$$p = \frac{\text{adj1(31)} \times \text{adj1(33)}}{1 + \text{adj1(31)} \times \text{adj1(33)}}. \tag{16}$$

In the above equation adj1(33) is defined as

$$\text{adj1(33)} = \frac{N_{\bar{b}_s}}{N_{m_s}}. \tag{17}$$

The quantities adj1(31) and adj1(33) are two free parameters to be fixed by fitting the experimental data. This combination loop is performed over the parton list until it is empty. If the empty of parton list is hard to reach, the remaining partons will attempt to rehadronize by string fragmentation [1].

We assume the three-momentum of the coalesced hadron is the sum of its constituent quark (antiquark) three-momentum. The extra energy (the part deviated from the conservation) is additionally counted into a specific array, left for sharing among partons and hadrons in the current list. The three-position of the coalesced hadron is the random summation of the three-position of its constituent quark (antiquark). The time of coalesced hadron is assumed to be the latest time among the constituent quarks (antiquarks).

Meanwhile, the phase-space constraint

$$\frac{16\pi^2}{9}\Delta r^3 \Delta p^3 = \frac{h^3}{d} \tag{18}$$

is considered. In the above equation the h^3/d is the volume occupied by a single hadron in the phase space, $d = 4$ refers to the spin and parity degeneracies of the hadron. The Δr and Δp stand for the sum of pair-wise relative distances between two (meson) or among three (baryon) partons in the spatial and momentum phase spaces, respectively. For details, one can refer to the program file coales_30.f.

The mesons and baryons considered are listed in Tables II and III, respectively. In the tables, the hadron proper probability is the expectation value (normalization factor) of its quark component wave function [49]. Only the hadron with nonzero proper probability can be the candidate in the coalescence hadronization. If the coalescing quarks (antiquarks) have same possibility to form a pseudoscalar meson or a vector meson (e.g., $u\bar{d}$ can coalesce into a π^+ or a ρ^+), then the one with less mass discrepancy between the (invariant) mass of coalescing quarks (antiquarks) and the mass of hadron will be preferred. And the same is true for the baryon production.

VIII. COMPARISON WITH EXPERIMENTS

A. High-energy reaction

In B- and C-simulation framework, if the hadronization is implemented by LSF, the key parameters are K, σ_G, α, and β [adj1(10), adj1(34), adj1(6), and adj1(7) in PACIAE, corresponding to PARP(31), PARJ(21), PARJ(41), and PARJ(42) in PYTHIA]. K is a multiplicative factor of hard scattering cross sections, as shown in Eq. (4). σ_G is the width of Gaussian p_x and p_y transverse momentum distributions for the primary hadrons [1]. α and β are the parameters in the Lund fragmentation function [1,50]:

$$f(z) \propto z^{-1}(1-z)^{\alpha} \exp\left(-\beta m_T^2/z\right), \tag{19}$$

where z is the fraction of energy taken by a hadron fragmented from a parton and $m_T^2 = m^2 + p_T^2$ is the transverse mass of the hadron. The σ_G, α, and β hence couple with each other.

On the other hand, if the coalescence hadronization model (Coal) is selected in C-simulation framework (note: in the B-simulation framework the hadronization is implemented by LSF only), the key parameters would be K, σ_q, e_{she} [adj1(10), adj1(34), adj1(7)], and adj1(16). Here K has the same meaning as mentioned above. σ_q and e_{she} are the width of the generated quark-antiquark p_T distribution in the energetic quark deexcitation and the threshold energy of deexcitation, respectively. The adj1(16) refers to the allowed maximum number of deexcitation generation ($D = 1$).

The midrapidity charged particle multiplicity density $dN_{ch}/d\eta$ are given in Table IV. Here we see the PACIAE model results well reproduce the experimental data from PHOBOS [51] and ALICE [52].

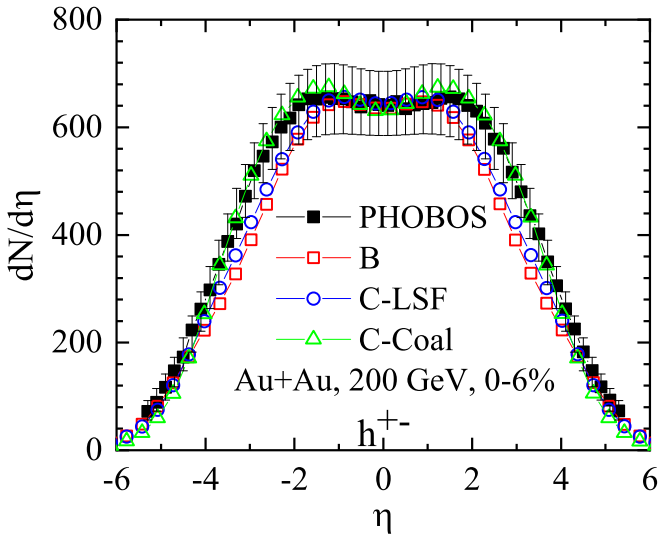

FIG. 7. Charged particle pseudorapidity distribution in 0%–6% most central Au + Au collisions at $\sqrt{s_{NN}} = 200$ GeV from PACIAE model simulations compared with PHOBOS data [53].

In the following figures, the simulated results from B-framework and C-framework with Lund string fragmentation as well as C-framework with coalescence model will be denoted as B, C-LSF, and C-Coal, respectively.

In Fig. 7, we compare the PHOBOS charged particle pseudorapidity distribution [53,54] (black solid squares) measured in 0%–6% most central Au + Au collisions at $\sqrt{s_{NN}} = 200$ GeV with B- and C-simulation framework results. The results of B-framework are indicated by red open squares, while the C-framework with LSF and Coal are, respectively, indicated by blue open circles and green open triangles. Figure 8 is the same as Fig. 7 but for the transverse-momentum spectrum. In the simulations, the parameters were tuned as follows:

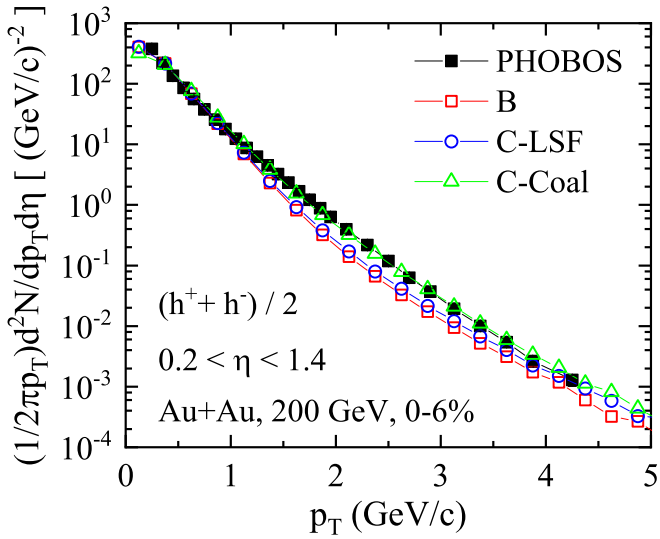

FIG. 8. Charged particle invariant transverse momentum spectra in 0%–6% most central Au + Au collisions at $\sqrt{s_{NN}} = 200$ GeV from PACIAE simulations compared with PHOBOS data [54].

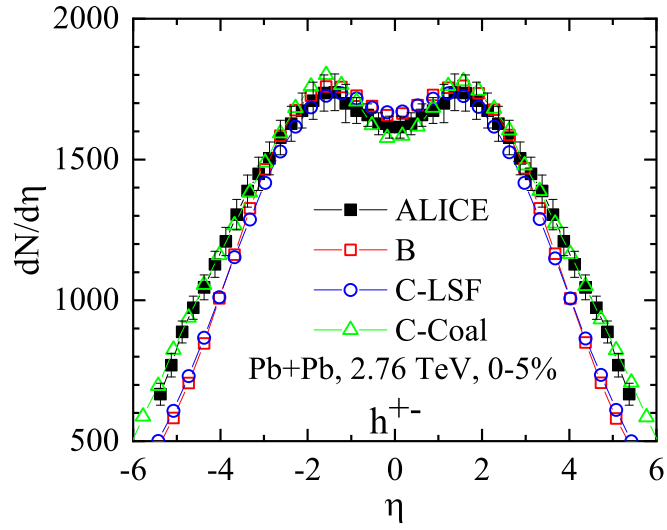

FIG. 9. Charged particle pseudorapidity distribution in 0%–5% most central Pb + Pb collisions at $\sqrt{s_{NN}} = 2.76$ TeV from PACIAE simulations compared with ALICE data [55].

(1) B-framework: $K = 0.9$, $\sigma_G = 0.45$, $\alpha = 0.3$, $\beta = 0.58$.
(2) C-framework LSF: $K = 2.5$, $\sigma_G = 0.45$, $\alpha = 0.3$, $\beta = 0.1$, and PARP(82) = 2.5.[1]
(3) C-framework Coal: $K = 0.7$, $\sigma_q = 0.6$, $e_{\rm she} = 1.8$, and PARP(91) = 1.3.[2]

One can see in these two figures that the PACIAE model well reproduces the PHOBOS data within the error bars.

A similar comparison with ALICE data measured in 0%–5% most central Pb + Pb collisions at $\sqrt{s_{NN}} = 2.76$ TeV is shown in Figs. 9 and 10. The parameters are

(1) B-framework: $K = 2.9$, $\sigma_G = 0.6$, $\alpha = 0.3$, $\beta = 0.13$.
(2) C-framework LSF: $K = 2.9$, $\sigma_G = 0.6$, $\alpha = 0.3$, $\beta = 0.012$.
(3) C-framework Coal: $K = 1.5$, $\sigma_q = 0.6$, $e_{\rm she} = 1.9$, and PARP(91) = 0.6.

Figures 9 and 10 show that the PACIAE model gives good descriptions of the ALICE charged particle pseudorapidity distribution [55] and p_T distribution data [56], except that the p_T distribution from C-Coal is slightly harder in the $p_T >$ 4 GeV/c region.

In Figs. 7 and 9, the pseudorapidity distributions from C-framework with coalescence model are wider than those from B- and C-framework with Lund string fragmentation regime at the region around $2 < |\eta| < 4$ for Au + Au collisions at $\sqrt{s_{NN}} = 200$ GeV and the region $|\eta| > 2$ for Pb + Pb collisions at $\sqrt{s_{NN}} = 2.76$ TeV. Also, in Figs. 8 and 10, the p_T distributions from the coalescence model are flatter than those from the Lund string fragmentation regime. It may stem

[1]The regularization scale of transverse-momentum spectrum for multiple interactions, parameter parp82 in PACIAE.

[2]The width of primordial transverse momentum $k_\perp$ for the partons inside the beam hadrons, parameter adj1(39) in PACIAE.

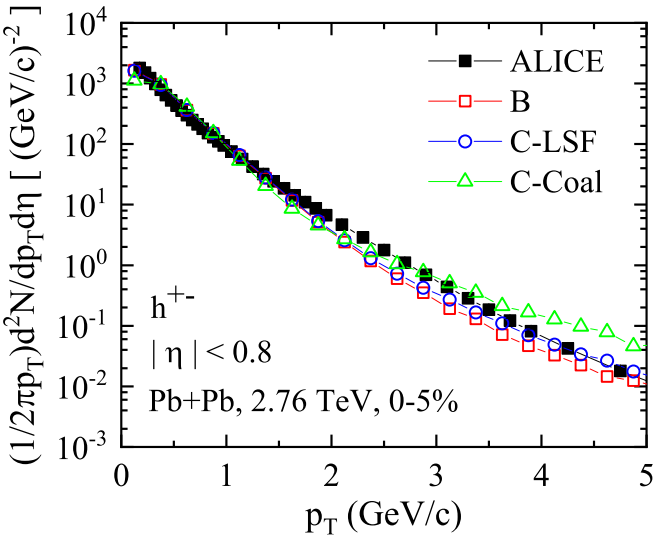

FIG. 10. Charged particle invariant transverse momentum spectra in 0%–5% most central Pb + Pb collisions at $\sqrt{s_{NN}} = 2.76$ TeV from PACIAE simulations compared with ALICE data [56].

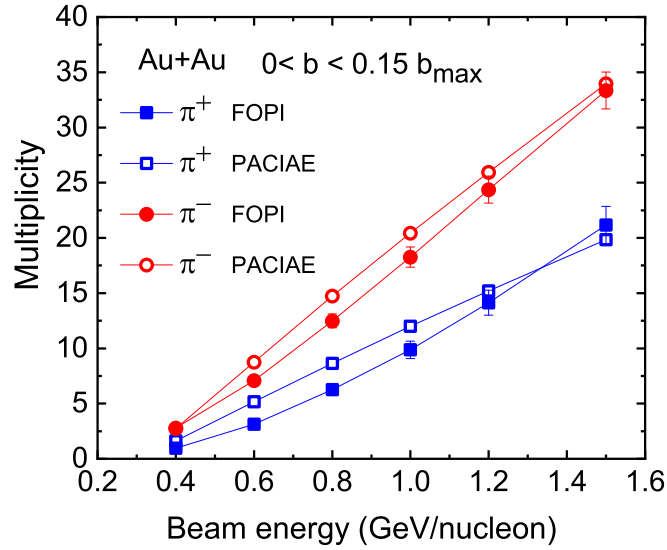

FIG. 11. The π^+ and π^- yields in most central Au + Au collisions at beam energies of 0.40, 0.60, 0.80, 1.0, 1.2, and 1.5 GeV/nucleon from PACIAE model simulations compared with the corresponding FOPI experimental data [59].

from the fact that, in the low- and intermediate-p_T regions, the partons tend to hadronize via coalescence mechanism, while the fragmentation is dominant in the higher-p_T region [44,46]. Moreover, due to the effect of partonic rescattering, one can see the results from the C-framework with Lund string fragmentation regime are slightly higher than those from the B-framework lacking the partonic rescattering. This partonic rescattering effect and the competition between different hadronization mechanisms need to be investigated in more detail in the next work.

B. Low-energy reaction

In the PACIAE A-simulation framework, there are two parameters only. One is the ratio of the inelastic to total cross section $R_{\text{inela/tot}}$ (x_ratio in program), another is the instantaneous decay probability of Δ particle (decpro in program). The $R_{\text{inela/tot}}$ is assumed to be a function of the incident channel $\sqrt{s_{NN}}$ [57,58]:

$$R_{\text{inela/tot}} = \frac{1.35(\sqrt{s_{NN}} - 2.015)^2}{0.015 + (\sqrt{s_{NN}} - 2.015)} \text{ if } \sqrt{s_{\text{NN}}} < 3\,\text{GeV}. \tag{20}$$

In Fig. 11, we compare PACIAE simulated results (decpro = 0.9) of π^+ and π^- yields to the corresponding FOPI experimental data [59] in most central Au + Au collisions at beam energy (fixed target) of 0.40, 0.60, 0.80, 1.0, 1.2, and 1.5 GeV/nucleon (corresponding to $\sqrt{s_{NN}}$ equal to 2.066, 2.155, 2.241, 2.402, and 2.520 GeV/nucleon, respectively). Here one sees that the results of the PACIAE model well reproduce the experimental data.

The PACIAE model results of π^+/p and π^-/p ratios are shown in Fig. 12 and compared with the FOPI experimental data measured in the same collision system as in Fig. 11. Since in the final hadronic state generated in the PYTHIA (PACIAE) model the light nuclei (d, t, ^{3}He, ^{4}He, Li, etc.) are not identified. The charge number of above light nuclei must first be added into the proton data and then compared with PACIAE results due to the charge-conservation principle. Figure 12 shows that the PACIAE results generally well reproduce the FOPI experimental data.

The E895 measured π^+ and π^- rapidity distributions [60] in 0%–5% most central Au + Au collisions at nominal beam energy of 2 GeV/nucleon are compared with PACIAE results in Fig. 13. The actual beam energy after correction for the energy loss is 1.85 GeV/nucleon, which corresponds to $\sqrt{s_{NN}} = 2.64$ GeV. One can see here that the E895-measured π^+ and π^- rapidity distributions are fairly well reproduced by PACIAE.

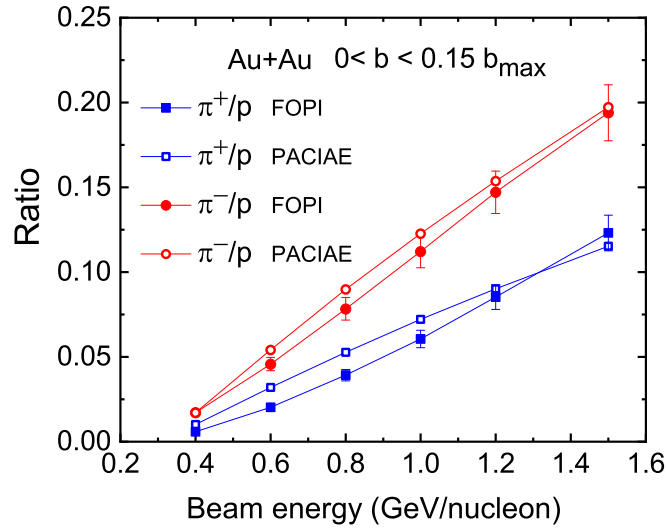

FIG. 12. The π^+/p and π^-/p ratios in most central Au + Au collisions at beam energies of 0.40, 0.60, 0.80, 1.0, 1.2, and 1.5 GeV/nucleon from PACIAE model simulations compared with the FOPI experimental data [59].

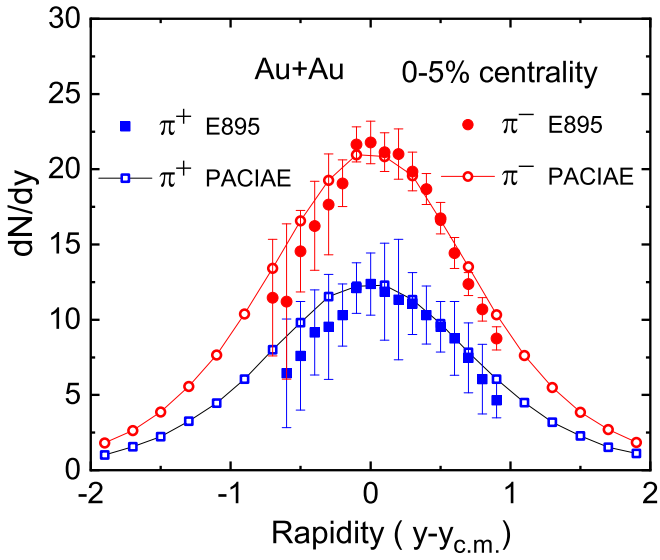

FIG. 13. The E895 π^+ and π^- experimental rapidity distributions in 0%–5% most central Au + Au collisions at 1.85 GeV/nucleon actual beam energy [60] compared with PACIAE model simulations.

Similarly, Fig. 14 gives the comparison of E895 measured π^+ and π^- transverse mass (transverse momentum) distributions [60] to the PACIAE results in the same collision system as in Fig. 13. One can see here that the experimentally measured π^+ and π^- transverse mass distributions are harder than PACIAE simulations in the transverse mass interval of $0.1 - 0.3$ GeV/c^2, otherwise softer than the PACIAE results. As the outgoing particle momentum in the low-energy A-framework simulation is fixed by the two-body scattering kinematic and there are no adjustable parameters, unlike that in the high-energy B- and C-framework simulations, the improvement of the agreement between experiment and theory in particle transverse mass distribution has to be studied further.

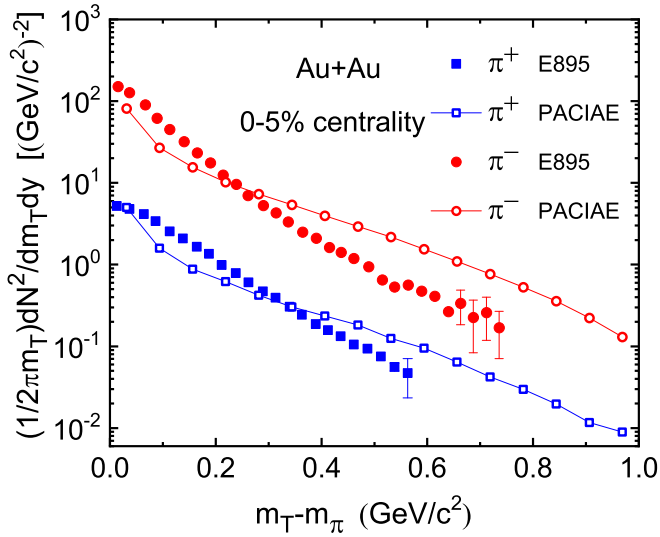

FIG. 14. The same as the Fig. 13 but for π^+ and π^- transverse mass distributions.

IX. SUMMARY AND CONCLUSION

We have constructed a phenomenological parton and hadron cascade model PACIAE 3.0 based on PYTHIA 6.428 and PACIAE 2.2 series for nuclear collisions. Besides the original simulation framework (renamed as C-simulation framework) for high-energy ($\sqrt{s_{NN}} \geqslant 3$ GeV) nuclear collisions, we design further a B-simulation framework for high-energy nuclear collisions and the A-simulation framework for the low-energy ($\sqrt{s_{NN}} < 3$ GeV) nuclear collisions. The C-simulation framework is a complete parton and hadron cascade simulation developed from initial partonic state to the partonic rescattering stage, the hadronization stage, and the hadronic rescattering stage. However, the partonic rescattering is not included in the B-simulation framework. As for the A-simulation framework, it is based on the hadronic two-body elastic- and inelastic-scattering kinematics in the hadronic degree of freedom only. On the other hand, the parton-parton inelastic scatterings are implemented, the single-string structure and multiple-string interaction mechanisms are introduced investigating the strangeness enhancement, and the phenomenological coalescence hadronization model is modified in the C-simulation framework. Finally, the particle yield, transverse momentum distribution, and rapidity distribution resulted from A-simulation framework well reproduce the data measured in the FOPI and E895 experiments, and the results from B- and C-simulation frameworks are entirely consistent with the data measured at the RHIC and LHC energies.

It seems necessary to introduce the mean field, Fermi motion, and Pauli blocking effects in the A-simulation framework for the study of symmetry energy and the equation of state. For the investigation of heavy flavor production in relativistic nuclear collisions with B- and/or C-simulation frameworks, it may be obliged to open the special channels for the "heavy flavors" sector in PYTHIA. It is a bias sampling method, the calculated results must be multiplied by a correcting (normalization) factor before comparison with experimental data.

At last, from a technical point of view, PACIAE 3.0 is written in FORTRAN programming language and based on PYTHIA 6. With the development of physics and computer science, high-energy community embraces more modern languages and technologies, in particular from FORTRAN to object-oriented C++ language. A plan of accessing to C++-based PYTHIA 8 [2] is one of our future goals and is on the timetable, in which we expect more fruitful physics to be integrated with PACIAE.

ACKNOWLEDGMENTS

We thank X.-M. Zhang, S.-S. Shi, and W.-C. Zhang for helpful discussions. This work was supported by the National Natural Science Foundation of China (Grants No. 12375135, No. 11775094, No. 11905188, No. 12275322) and the 111 project of the foreign expert bureau of China. Yu-Liang Yan acknowledges the financial support from Key Laboratory of

TABLE V. Object of study vs switch and/or parameter.

Simulation mode	iMode[a] = 1: A-simulation framework; =2: B-simulation framework;
–	=3: C-simulation framework
QCD subprocesses selection	nchan = 0: inelastic (INEL); = 1: non-single diffractive (NSD); = 2: Drell-Yan;
–	= 3: J/ψ production; = 4: heavy-flavor production; = 5: direct photon; = 6: soft only;
–	= 7: $W^{+/-}$ production; = 8: default PYTHIA; = 9: Z^0 production
Chiral magnetic effect	adj1(3)=0: off; =1, on
Hadronization model	adj1(12) = 0: Lund string fragmentation model; = 1: coalescence model
Parton rescattering	adj1(1) > 0: with; = 0: without.
–	adj1(1) is a factor multiplying on parton-parton cross section
	iparres = 0: elastic processes only;
Process in parton rescattering	= 1: elastic + inelastic processes.
	i_inel_proc = 6: with inelastic process of 4, 6, and 7;
	= 7: with inelastic process 7 only
Lund string fragmentation model	adj1(10): K factor, adj1(6): α, adj1(7): β, adj1(34): σ_H
	adj1(16): allowed number of deexcitation generation,
Coalescence model	adj1(17): threshold energy of deexcitation,
	adj1(29): deexcitation function,
	adj1(34): σ_q
	kjp22 = 1: variable single string tension;
Effective string tension	= 2: variable multiple string tension;
	= 3: variable single + multiple string tension;
	= 4: constant string tension
Hadron rescattering	kjp21 = 1: with; =0: without

[a]Name in program (the same later).

Quark and Lepton Physics in Central China Normal University (Grant No. QLPL201805) and the Continuous Basic Scientific Research Project (Grant No. WDJC-2019-13).

APPENDIX: PACIAE 3.0 USER'S GUIDE

1. Program running

To run PACIAE 3.0, one direct way is to compile the source code, modify the input file usu.dat as needed and execute the program. Another way is to use the toy SHELL script PACIAE.sh. A makefile has been integrated in the PACIAE.sh with the GFortran compiler specified. It will compile the source code, generate usu.dat (the old usu.dat will be overwritten) and run the program automatically. More details can be found in the README.md file.

PACIAE 3.0 comes with a simple internal on-line analyzing module and outputs several files. The analyzing output file is rms.out, where some basic results of collisions and six distributions (rapidity distribution dN/dy, invariant transverse momentum spectrum $(1/p_T)dN/dp_T$, pseudorapidity distribution $dN/d\eta$, invariant transverse mass spectrum $(1/m_T)dN/dm_T$, event-wise multiplicity distribution, and transverse momentum spectrum dN/dp_T) are provided. The rms0.out is a file recording the input parameters. The main.out file is PYTHIA-style particle list output file. If the user chooses to output OSCAR-format files, there will be an oscar.out file that records list of final-state particles or full event history.

2. The basic tuning criteria

In Sec. VIII, we give rough tuning results at both low and high energies. A tune essentially requires a very large amount of experimental data fitting with a couple of adjustment parameters, such as the Perugia 2011 tune of PYTHIA 6 [61] and Monash 2013 tune of PYTHIA 8 [62] that ALICE typically used. However, for heavy-ion collisions, it is impossible to meet a "perfect" tune due to our inadequate understanding of this very sophisticated large system. A recommended effective tuning criterion is as follows: Fit the midrapidity density, pseudorapidity distributions, and/or transverse momentum spectra of basic charged particles to the experimental data at the corresponding system and energy. Then one could conduct other studies of interest. Another criterion is based on what one would like to study. For instance, to study the topic of nuclear modification factors R_{AA}, one can fit the R_{AA} of $\pi^{\pm}$ to experimental data at first [63].

3. Incident channel selection in the update of *hh* collision list

The particle yield in the final hadronic state is sensitively depended on the selection of incident channel in

the update of *hh* collision list after each *hh* collision. Presently, only the *NN* collision is selected at the beginning of *hh* simulation loop and in the subroutine of updtlp, updatl, and intdis consistently in the B- and C-simulation frameworks. In the A-simulation framework, only the *NN*, ΔN, and πN are selected at the beginning of *hh* collision simulation loop and in the subroutines updatl_nn and intdis consistently.

4. Main switches and parameters

In the follows we list main switches and parameters as well as their potentials, respectively, for user reference. As mentioned above the decpro and x_ratio are the only two free parameters in the A-simulation framework, thus the following Table V is just for the B- and C-simulation frameworks only. More details could be found in usu.dat, PACIAE.sh, and the comments in main_30.f.

[1] T. Sjöstrand, S. Mrenna, and P. Z. Skands, J. High Energy Phys. 05 (2006) 026.
[2] C. Bierlich *et al.*, SciPost Phys. Codebases **8** (2022).
[3] G. Corcella, I. G. Knowles, G. Marchesini, S. Moretti, K. Odagiri, P. Richardson, M. H. Seymour, and B. R. Webber, J. High Energy Phys. 01 (2001) 010.
[4] T. Gleisberg, S. Hoeche, F. Krauss, M. Schonherr, S. Schumann, F. Siegert, and J. Winter, J. High Energy Phys. 02 (2009) 007.
[5] K. Geiger and B. Muller, Nucl. Phys. B **369**, 600 (1992).
[6] X.-N. Wang and M. Gyulassy, Phys. Rev. D: Part. Fields **44**, 3501 (1991).
[7] N. S. Amelin, L. V. Bravina, L. P. Csernai, V. D. Toneev, K. K. Gudima, and S. Y. Sivoklokov, Phys. Rev. C **47**, 2299 (1993).
[8] S. A. Bass *et al.*, Prog. Part. Nucl. Phys. **41**, 255 (1998).
[9] Z.-W. Lin, C. M. Ko, B.-A. Li, B. Zhang, and S. Pal, Phys. Rev. C **72**, 064901 (2005).
[10] B.-H. Sa, D.-M. Zhou, Y.-L. Yan, X.-M. Li, S.-Q. Feng, B.-G. Dong, and X. Cai, Comput. Phys. Commun. **183**, 333 (2012).
[11] A. Kisiel, T. Taluc, W. Broniowski, and W. Florkowski, Comput. Phys. Commun. **174**, 669 (2006).
[12] W. Cassing and E. L. Bratkovskaya, Nucl. Phys. A **831**, 215 (2009).
[13] T. Pierog, I. Karpenko, J. M. Katzy, E. Yatsenko, and K. Werner, Phys. Rev. C **92**, 034906 (2015).
[14] J. Weil *et al.* (SMASH Collaboration), Phys. Rev. C **94**, 054905 (2016).
[15] K. Kauder (JETSCAPE Collaboration), Nucl. Phys. A **982**, 615 (2019).
[16] C. Bierlich, G. Gustafson, L. Lönnblad, and H. Shah, J. High Energy Phys. 10 (2018) 134.
[17] Y.-X. Zhang *et al.* (TMEP Collaboration), Phys. Rev. C **97**, 034625 (2018).
[18] H. Wolter *et al.* (TMEP Collaboration), Prog. Part. Nucl. Phys. **125**, 103962 (2022).
[19] G.-C. Yong, Phys. Rev. C **96**, 044605 (2017).
[20] D.-M. Zhou, Y.-L. Yan, X.-L. Li, X.-M. Li, B.-G. Dong, X. Cai, and B.-H. Sa, Comput. Phys. Commun. **193**, 89 (2015).
[21] Y.-L. Yan, D.-M. Zhou, X. Cai, and B.-H. Sa, Comput. Phys. Commun. **224**, 417 (2018).
[22] Z.-L. She, D.-M. Zhou, Y.-L. Yan, L. Zheng, H.-g. Xu, G. Chen, and B.-H. Sa, Comput. Phys. Commun. **274**, 108289 (2022).
[23] Y.-L. Yan, D.-M. Zhou, A.-K. Lei, X.-M. Li, X.-M. Zhang, L. Zheng, G. Chen, X. Cai, and B.-H. Sa, Comput. Phys. Commun. **284**, 108615 (2023).
[24] B. H. Sa and A. Tai, Comput. Phys. Commun. **90**, 121 (1995).
[25] A. Tai and B.-H. Sa, Comput. Phys. Commun. **116**, 353 (1999).
[26] B. Andersson, A. Tai, and B.-H. Sa, Z. Phys. C: Part. Fields **70**, 499 (1996).
[27] B.-H. Sa, X. Cai, Z. D. Su, A. Tai, and D.-M. Zhou, Phys. Rev. C **66**, 044902 (2002).
[28] H. Pi, Comput. Phys. Commun. **71**, 173 (1992).
[29] T. Sjöstrand, Comput. Phys. Commun. **82**, 74 (1994).
[30] T. Sjöstrand and M. Utheim, Eur. Phys. J. C **80**, 907 (2020).
[31] E. M. Levin and L. L. Frankfurt, JETP Lett. **2**, 65 (1965).
[32] S. Acharya *et al.* (ALICE Collaboration), ALICE-PUBLIC-2018-011 (2018).
[33] https://github.com/ArcsaberHep/PACIAE.
[34] https://gitee.com/arcsaberhep/PACIAE.
[35] B.-H. Sa, D.-M. Zhou, Y.-L. Yan, B.-G. Dong, and X. Cai, Comput. Phys. Commun. **184**, 1476 (2013).
[36] B. L. Combridge, J. Kripfganz, and J. Ranft, Phys. Lett. B **70**, 234 (1977).
[37] R. D. Field, *Applications Of Perturbative QCD* (Addison-Wesley Publishing Company, Inc., New York, 1989).
[38] J. Adam *et al.* (ALICE Collaboration), Nat. Phys. **13**, 535 (2017).
[39] A. Tai and S. Ben-Hao, Phys. Lett. B **409**, 393 (1997).
[40] L. Zheng, D.-M. Zhou, Z.-B. Yin, Y.-L. Yan, G. Chen, X. Cai, and B.-H. Sa, Phys. Rev. C **98**, 034917 (2018).
[41] D.-M. Zhou, L. Zheng, Z.-H. Song, Y.-L. Yan, G. Chen, X.-M. Li, X. Cai, and B.-H. Sa, Phys. Rev. C **102**, 044903 (2020).
[42] N. Fischer and T. Sjöstrand, J. High Energy Phys. 01 (2017) 140.
[43] R. C. Hwa and C. B. Yang, Phys. Rev. C **67**, 034902 (2003).
[44] V. Greco, C. M. Ko, and P. Levai, Phys. Rev. Lett. **90**, 202302 (2003).
[45] V. Greco, C. M. Ko, and P. Levai, Phys. Rev. C **68**, 034904 (2003).
[46] R. J. Fries, B. Müller, C. Nonaka, and S. A. Bass, Phys. Rev. Lett. **90**, 202303 (2003).
[47] R. J. Fries, B. Müller, C. Nonaka, and S. A. Bass, Phys. Rev. C **68**, 044902 (2003).
[48] F.-L. Shao, Q.-B. Xie, and Q. Wang, Phys. Rev. C **71**, 044903 (2005).
[49] H. Georgi, *Lie Algebras In Particle Physics: From Isospin To Unified Theories* (CRC Press, Taylor & Francis, Boca Raton, 2000).
[50] B. Andersson, G. Gustafson, and B. Soderberg, Z. Phys. C: Part. Fields **20**, 317 (1983).
[51] B. Alver *et al.* (PHOBOS Collaboration), Phys. Rev. C **83**, 024913 (2011).
[52] K. Aamodt *et al.* (ALICE Collaboration), Phys. Rev. Lett. **106**, 032301 (2011).
[53] B. B. Back *et al.*, Phys. Rev. Lett. **91**, 052303 (2003).
[54] B. B. Back *et al.* (PHOBOS Collaboration), Phys. Lett. B **578**, 297 (2004).
[55] E. Abbas *et al.* (ALICE Collaboration), Phys. Lett. B **726**, 610 (2013).

[56] B. Abelev *et al.* (ALICE Collaboration), Phys. Lett. B **720**, 52 (2013).
[57] G. F. Bertsch and S. Das Gupta, Phys. Rep. **160**, 189 (1988).
[58] J. Cugnon, T. Mizutani, and J. Vandermeulen, Nucl. Phys. A **352**, 505 (1981).
[59] W. Reisdorf *et al.* (FOPI Collaboration), Nucl. Phys. A **848**, 366 (2010).
[60] J. L. Klay *et al.* (E-0895 Collaboration), Phys. Rev. C **68**, 054905 (2003).
[61] P. Z. Skands, Phys. Rev. D **82**, 074018 (2010).
[62] P. Skands, S. Carrazza, and J. Rojo, Eur. Phys. J. C **74**, 3024 (2014).
[63] B.-H. Sa, D.-M. Zhou, Y.-L. Yan, W.-D. Liu, S.-Y. Hu, X.-M. Li, L. Zheng, G. Chen, and X. Cai, J. Phys. G **49**, 065104 (2022).